PERGAMON

Vision Research 40 (2000) 1801–1811

Vision Research

www.elsevier.com/locate/visres

Center surround receptive field structure of cone bipolar cells in primate retina

Dennis Dacey [a,*], Orin S. Packer [a], Lisa Diller [a], David Brainard [b], Beth Peterson [a], Barry Lee [c]

[a] *Department of Biological Structure, University of Washington, Box 357420, Seattle, WA 98195-7420, USA*
[b] *Department of Psychology, University of California Santa Barbara, Santa Barbara, CA, USA*
[c] *Max Planck Institute for Biophysical Chemistry, Gottingen, Germany*

Received 28 September 1999; received in revised form 5 January 2000

Abstract

In non-mammalian vertebrates, retinal bipolar cells show center-surround receptive field organization. In mammals, recordings from bipolar cells are rare and have not revealed a clear surround. Here we report center-surround receptive fields of identified cone bipolar cells in the macaque monkey retina. In the peripheral retina, cone bipolar cell nuclei were labeled in vitro with diamidino-phenylindole (DAPI), targeted for recording under microscopic control, and anatomically identified by intracellular staining. Identified cells included 'diffuse' bipolar cells, which contact multiple cones, and 'midget' bipolar cells, which contact a single cone. Responses to flickering spots and annuli revealed a clear surround: both hyperpolarizing (OFF) and depolarizing (ON) cells responded with reversed polarity to annular stimuli. Center and surround dimensions were calculated for 12 bipolar cells from the spatial frequency response to drifting, sinusoidal luminance modulated gratings. The frequency response was bandpass and well fit by a difference of Gaussians receptive field model. Center diameters were all two to three times larger than known dendritic tree diameters for both diffuse and midget bipolar cells in the retinal periphery. In one instance intracellular staining revealed tracer spread between a recorded cell and its nearest neighbors, suggesting that homotypic electrical coupling may contribute to receptive field center size. Surrounds were around ten times larger in diameter than centers and in most cases the ratio of center to surround strength was ~ 1. We suggest that the center-surround receptive fields of the major primate ganglion cell types are established at the bipolar cell, probably by the circuitry of the outer retina.

Keywords: Bipolar cell; Receptive field; Retina; Primate

1. Introduction

It has been known for over 40 years that the vertebrate retina utilizes lateral inhibition to create spatially opponent center-surround receptive fields. The fundamental significance of center-surround organization for efficient signal coding at the earliest stages in the visual process has been treated theoretically (e.g. Barlow, 1961; Srinivasan, Laughlin & Dubs, 1982) yet the precise origins of spatial opponency are still not fully understood. In both mammalian (Kuffler, 1953) and non-mammalian (Barlow, 1953) retina, ganglion cells show center-surround receptive fields. Receptive field surrounds are also found in non-mammalian bipolar cells (Werblin & Dowling, 1969; Matsumoto & Naka, 1972; Kaneko, 1973; Schwartz, 1974), and it is reasonably well established that the bipolar cell surround originates, at least in part, via a horizontal cell feedback pathway that gives rise to a surround in the photoreceptors themselves (reviews: Burkhardt, 1993; Kamermans & Spekreijse, 1999).

In mammals by contrast, there is little direct evidence for a surround at the bipolar cell level. Current injections made into rabbit horizontal cells affected the surround contribution to the ganglion cell light response (Mangel, 1991). In the developing rabbit retina

* Corresponding author. Tel.: +1-206-543-0224; fax: +1-206-543-1524.
E-mail address: dmd@u.washington.edu (D. Dacey)

0042-6989/00/$ - see front matter
PII: S0042-6989(00)00039-0

some spatial antagonism in retinal interneurons presumed to be cone bipolar cells was observed (Dacheux & Miller, 1981) but these cells were not morphologically identified. A possible surround contribution to a rabbit rod bipolar cell light response may also have been observed but the recording was too brief to address this question with the appropriate stimuli (Dacheux & Raviola, 1986). In cat retina, cone bipolar cells showed little spatial opponency (Nelson, Kolb, Robinson & Mariani, 1981; Nelson & Kolb, 1983), suggesting that in mammals the ganglion cell surround may be largely determined in the inner retina via the long range inhibitory connections of amacrine cells. Consistent with this suggestion at least some ganglion cell surrounds appear to be generated mainly in the inner retina by spiking, wide field amacrine cells (Taylor, 1999).

Here we report measurements of strong center-surround receptive field organization in a sample of morphologically identified cone bipolar cells in macaque monkey using an in vitro preparation of the intact retina (Dacey, 1999). Nine distinct types of primate cone bipolar cells have been recognized in previous anatomical studies. 'Midget' bipolar cells (Polyak, 1941; Boycott & Dowling, 1969; Kolb & Dekorver, 1991; Calkins, Schein, Tsukamoto & Sterling, 1994) form two distinct populations that largely contact single cones: flat midget bipolar cells make non-invaginating or basal contacts with the cone pedicle and terminate in the outer portion of the inner plexiform layer; invaginating midget bipolar cells extend dendritic tips into the pedicle and terminate in the inner portion of the inner plexiform layer. 'Diffuse' cone bipolar cells non-selectively contact multiple cones but can be divided into six distinct populations by discrete levels of axonal stratification in the inner plexiform layer (Polyak, 1941; Boycott & Dowling, 1969; Boycott & Wässle, 1991; Grünert, Martin & Wässle, 1994). Finally a single 'blue cone' bipolar cell type selectively contacts short wavelength sensitive cones (Mariani, 1984; Kouyama & Marshak, 1992). The present results include examples from both midget and diffuse bipolar cell classes and, for all cells recorded, a clear surround component much like that classically observed in non-mammalian retina was observed.

2. Methods

2.1. In vitro preparation and histology

The in vitro preparation of macaque retina has been previously described (Dacey & Lee, 1994; Dacey, Lee, Stafford, Pokorny & Smith, 1996). Eyes from *Macaca fascicularis* ($n = 2$), *M. nemestrina* ($n = 10$) and *Papio c. anubis* ($n = 2$) were obtained from the tissue program of the Washington Regional Primate Research Center. The retina, choroid, and pigment epithelium were dissected free of the vitreous and sclera in oxygenated culture medium (Ames' Medium, Sigma) and placed flat, vitreal surface up, in a superfusion chamber mounted on the stage of a light microscope. Cone bipolar cell nuclei were identified in the inner nuclear layer using the nuclear stain 4,6 diamidino-2-phenylindole (DAPI) (10 μM). For combined intracellular recording and staining, microelectrodes (impedances ~ 200–300 MΩ) were filled with a solution of 3% Neurobiotin (Vector Labs, Burlingame, CA) and 2% pyranine (Molecular Probes, Eugene, OR) in 1 M KCL. Pyranine fluorescence in the electrode and DAPI fluorescence in cells were viewed together under episcopic illumination with the same filter combination. Following cell penetration cone bipolar cell identity was confirmed in vitro by observing dendritic and axonal morphology after iontophoresis of pyranine into the cell.

After recording, cells were injected with Neurobiotin ($+0.1$ -0.3 nA; ~15 min). Retinas were dissected free of the choroid, fixed in phosphate buffered (0.1 M, pH 7.4) 4% paraformaldehyde for ~2 h, rinsed in 0.1 M phosphate buffer, and placed in a buffered solution of 0.1% Triton X-100 (Sigma) containing the Vector avidin–biotin–HRP complex (Vector Laboratories, Burlingame, CA) for 5 h or overnight. Retinas were rinsed for 2 h and standard horseradish peroxidase (HRP) immunohistochemistry was performed using diaminobenzidine (DAB) (Kirkegaard & Perry Laboratories, Gaithersburg, MD) as the chromogen. Retinas were mounted on a slide in a water-based solution of polyvinyl alcohol and glycerol to prevent tissue shrinkage.

2.2. Light stimuli

Two methods were used to project light stimuli onto the retina. The first method used a light emitting diode (LED) based stimulator (Dacey & Lee, 1994; Dacey et al., 1996). Red, green and blue (peak wavelengths of 652, 525 and 460 nm, respectively) LEDs and associated optics were mounted vertically and positioned above the microscope such that the light path was projected through the camera port onto the retina surface. A joystick controlling a motorized micropositioner was used to adjust the position of a small test spot (~40 μm diameter) on the receptive field until a maximum response amplitude was observed. Larger apertures were then used to project 200 or 1000 μm diameter white spots onto the retina. The spots were square wave modulated (100% luminance contrast) at either 1.22 or 2.44 Hz. Light levels were in the mid photopic range; an equivalent value in trolands (td) was estimated at 1000 (Dacey et al., 1996).

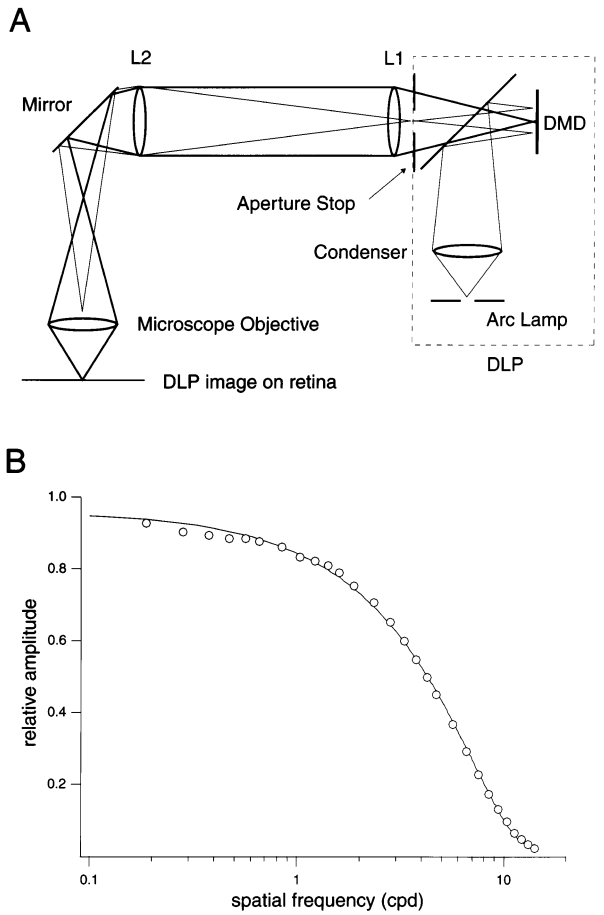

Fig. 1. (A) Simplified optical diagram of the DLP-based visual stimulator. Light from a zenon arc lamp is divided into parallel red, green and blue channels, one of which is illustrated to the right of the aperture stop in the diagram. Each channel has its own 'Digital Micromirror Device' (DMD). The DMD is an array of tiny mirrors each of which can be tipped into an 'on' position (light reflected into the optics) or an 'off' position (light reflected into a light trap). An image is formed by turning on the appropriate mirrors. After being reflected from the DMD, light from the three channels is recombined into a single coaxial beam (thin rays in diagram) so that an image of the source is formed in the plane of the aperture. Lens L2 images the source in the back focal plane of the objective causing it to be out of focus in the plane of the retina. This produces a stimulus of uniform intensity. The aperture reduced the numerical aperture of the stimulator to 0.01, sufficiently small so that the image of the stimulus was acceptably sharp if the plane of focus was within 100 μm of the inner segment apertures of the photoreceptors. An image of the DMD (thick rays) was formed in the rear image plane of the microscope objective (4×) by lenses L1 and L2. The microscope objective then reimages the DMDs on the retina. The focal lengths of L1 and L2 were chosen so that each of the mirrors of the DMD subtended ~3 μm on the retina. The field of view was 1.8 × 2.4 mm. (B) The optical modulation transfer function (MTF) of the spatial light stimulator. The MTF was measured by drifting sine wave gratings of increasing spatial frequency across a 6 μm aperture and measuring the transmitted light with a photocell. This MTF has been corrected for contrast losses caused by the finite size of the 6 μm aperture. Solid line through the data points was fit by eye. Spatial frequency is given as cycles per degree (cpd) of visual angle for the macaque monkey eye (1° = 200 μm on the retina).

The second method employed a visual display generator (Cambridge Research Systems VSG Series 3) to drive a digital light projector (DLP; Electrohome, Vistapro Plus). The DLP is based on a recently introduced digital display technology; details of the optical design together with an overall evaluation of this technology will be given elsewhere (Packer, Diller, Brainard & Dacey, 2000). In brief, images created by the display generator were projected through the camera port of the microscope to the retinal image plane via simple relay optics (Fig. 1A); a 4× microscope objective lens was used to give a final image size on the retina of 2.4 × 1.8 mm (at this magnification each pixel in the projector's display subtended 3 μm in the plane of the retina).

Using the DLP-based visual stimulator, three classes of spatial stimuli were used to characterize the structure of the cone bipolar cell receptive field: (1) flickering spots of varying diameter; (2) flickering annuli of varying inner diameter; and (3) drifting sinusoidally modulated gratings of varying spatial frequency. For each spatial type, a series of stimuli was presented and the cell's response was measured as a function of the spatial parameter. Within a series, the modulation contrast (100%) and temporal frequency (2, 4 or 10 Hz) were held fixed. All stimulus modulations were isochromatic (CIE 1931 chromaticity $x = 0.304$, $y = 0.349$) around a background with the same chromaticity and a mean luminance of ~1000 td. Spot and annular stimuli were centered on the cell's receptive field by systematically moving small flickering spots over the receptive field and locating the position that elicited a peak response.

2.3. Data acquisition

The intracellular voltage was amplified (Axon Instruments, Axoprobe-1A) and digitized (National Instruments, NB-MIO16) at a rate of 10 kHz. The acquired data was then averaged over multiple temporal cycles of stimulus presentation (typically 10–20). The number of stimulus cycles over which the data was averaged was always several times greater than the temporal frequency of the stimulus. Fourier analysis was used to determine the amplitude and phase of the cell's response at the temporal frequency of the stimulus modulation.

2.4. Model

Response amplitudes and phases to series of spatial stimuli (either spots, annuli, or gratings) were used to determine the parameters of a difference of Gaussians receptive field model (Rodieck & Stone, 1965). The model specifies the spatial profile of both center and surround as a circularly-symmetric Gaussian. The strength of the center and surround vary separately, and the model allows for a difference in response phase

between the center and surround mechanism (Enroth-Cugell, Robson, Schweitzer-Tong & Watson, 1983). The receptive field center has a radial profile $C(r)$ given by

$$C(r) = W_c \cdot \frac{1}{\pi} \cdot \left(\frac{1}{R_c}\right)^2 \cdot e^{(-r/R_c)^2} \quad (1)$$

where W_c specifies the strength of the center and R_c specifies the size of the center (the radius where sensitivity has fallen by a factor of 1/e from its peak). A similar expression defines the radial profile of the surround $S(r)$, with strength W_s and radius R_s. The amplitude of center and surround response to a stimulus modulation is given by computing the two-dimensional spatial integral of the product of the appropriate receptive field and stimulus profiles. For the case of drifting gratings, the computation can be performed by noting that a drifting grating is the sum of two counterphase flickering gratings in spatial and temporal quadrature.

The overall amplitude and phase of the cell's response is obtained by combining center and surround responses:

$$R = (A_c \cdot e^{(i \cdot \theta_c)}) + (A_s \cdot e^{(i \cdot \theta_s)}) = A \cdot e^{(i \cdot \theta)} \quad (2)$$

where A_c and A_s represent the amplitudes of center and surround responses and θ_c and θ_s represent the phases of their responses at the temporal frequency of the stimulus modulation. Because the centering of the stimuli with respect to receptive field locations was not always performed before the presentation of drifting gratings, and because the precision of the centering procedure was limited, an additional parameter was added to the model to account for a possible spatial offset. For the case of drifting gratings, this parameter allowed the model to account for spatial frequency dependent phase shifts that arise when the grating is not in cosine phase with the receptive field at the start of a stimulus cycle.

Numerical search (Grace, 1990) was used to find the model parameters that provided the best account of the responses for each series of spatial data. The error function minimized was the mean square difference between predicted and measured responses, expressed in the complex domain. If used in an automated fashion, the numerical search procedure often returned parameters that produced a poor fit to the data. Therefore an iterative fitting procedure was adopted in which the operator set initial fitting parameters to facilitate identification of values that provide a good fit.

To assess the optical quality of the DLP-based visual stimulator, we measured its spatial frequency dependent contrast. A 6 μm diameter aperture was placed in front of a silicon photodiode at the location occupied by the retina. Fig. 1B shows the response of this 'artificial cell' to drifting gratings as a function of spatial frequency. The amplitudes have been corrected for the blur caused by the aperture and therefore represent the optical attenuation of the visual stimulator. It is clear from Fig. 1B that the stimulator itself attenuates stimulus contrast as a function of spatial frequency. The data were corrected for this loss on the assumption that the contrast response function was linear. As discussed in Section 2, for the relatively large receptive fields studied here, this correction had little effect on the model parameter estimates.

3. Results

3.1. Cell identification

Microscopically targeted and pyranine filled cells that showed branching dendritic trees and multiple cone contacts were identified as diffuse bipolar cells. As expected, cells with axonal branching in the outer or inner portions of the inner plexiform layer showed, respectively, hyperpolarizing or depolarizing light responses to small flickering spots centered on the receptive field. Because the aim of this initial study was to report on the general spatial organization of the bipolar cell receptive field, no attempt was made to further divide the ON and OFF diffuse bipolar cells in our sample into one of the six types distinguished by axonal stratification (Boycott & Wässle, 1991). Using Neurobiotin injection and subsequent HRP histochemistry, we were able to recover the morphology of five cells in which a recorded cell was identified as a diffuse bipolar cell by pyranine staining in vitro. A Neurobiotin-labeled ON-center diffuse cone bipolar cell is shown at three levels of focus in the photomicrographs of Fig. 2. The cell had an axon arbor about 40 μm in diameter located in the inner portion of the inner plexiform layer (Fig. 2A) and cell body in the middle of the inner nuclear layer (arrow in Fig. 2B). The dendritic tree in the outer plexiform layer (Fig. 2C) was similar in diameter to the axon arbor. The somas of several nearby bipolar cells were also filled with Neurobiotin following injection into the center cell (arrowheads in Fig. 2B). The regular, mosaic-like spacing of these lightly labeled cells suggests that they are neighboring cells of the same type (Milam, Dacey & Dizhoor, 1993). Five midget bipolar cells were also identified by pyranine staining and two of these were also recovered by HRP staining; the light response of one of these cells is illustrated in Fig. 4.

3.2. Spots and annuli reveal center-surround receptive fields

When the bipolar cell response to small and large diameter LED generated spot stimuli were compared, a strong surround component was revealed in all iden-

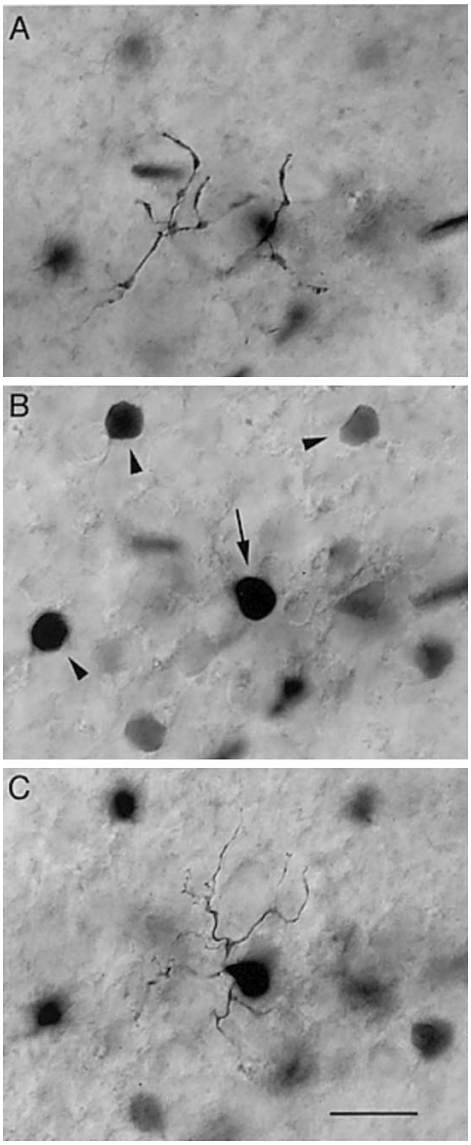

Fig. 2. Photomicrographs of a Neurobiotin-labeled ON-center diffuse bipolar cell. (A) Level of focus shows the 40 μm diameter axonal arbor in the inner plexiform layer. (B) Arrow indicates the cell body located in the inner nuclear layer. Cell bodies of neighboring bipolar cells labeled following injection of Neurobiotin into the center cell are also shown (arrowheads). (C) Level of focus is on the dendritic tree in the outer plexiform layer. Scale bar = 20 μm.

tified cone bipolar cells ($n = 11$: 8 OFF-center diffuse; 2 ON-center diffuse; 1 ON-center midget). The responses of two OFF-center cells are shown in Fig. 3A,B. Both cells hyperpolarized to a small 200 μm diameter spot (upper traces) and depolarized to a 1000 μm spot (lower traces). Responses of an ON-center cell are shown in Fig. 3C; this cell depolarized to the 200 μm spot (upper trace) and hyperpolarized to the 1000 μm spot (lower trace). For a few cells a complete reversal in response polarity to the large spot was not observed but center-surround interaction remained clearly evident in a more complex, biphasic waveform. The powerful effect of the surround to essentially reverse the response polarity when the stimulus diameter was increased dramatically revealed the bipolar cell surround. However, because the 200 μm diameter spot was presented first, on a black background, followed by the 1000 μm full field spot, this type of stimulus would tend to first desensitize the center relative to the surround, eliciting a relatively strong surround response.

An unequivocal demonstration of a receptive field surround was obtained when the DLP-based visual stimulator was employed to create more complex spatial stimuli (see Section 2). Spots and annuli were centered on the receptive field and presented on a steady background of the same mean luminance thereby minimizing any desensitizing effects of the stimuli. The response to such stimuli of an OFF-center, single-cone-contacting midget bipolar cell recorded in the nasal periphery is shown in Fig. 4. The cell hyperpolarized to modulation of a small spot (diameter = 150 μm) that was centered on the receptive field (Fig. 4A) and depolarized to an annulus (inner diameter = 150 μm; outer diameter = 1200 μm) that modulated only the receptive field surround (Fig. 4B).

3.3. Spatial properties of center-surround receptive fields

Three types of stimuli were used to further characterize the spatial properties of the cone bipolar cell receptive field and are illustrated together in Fig. 4C–E for the same midget bipolar cell shown in Fig. 4A,B. First, flickering spots of increasing diameter were presented on a steady background. Initially, response amplitude increased with increasing spot size and peaked at a spot diameter that strongly modulated the receptive field center (Fig. 4C, upper plot). Further increases in spot size increasingly modulated the receptive field surround and resulted in a decrease in response amplitude, reaching a plateau when the entire receptive field was modulated. The increasing surround contribution with increasing spot diameter also produced a gradual phase shift in the cell's response (Fig. 4C, lower plot). This phase shift was not as drastic as the nearly 180° shift in polarity seen in Fig. 3, where the center response was desensitized by the small spot and resulted in a greatly enhanced surround response to the larger spot. In Fig. 4C, the steady background minimized any desensitizing effects of the stimuli; both the center and surround contribute to the response at all spot sizes, with the surround increasing stimulated as spot size increases.

Second, flickering annuli of increasing inner diameter were presented (Fig. 4D). Initially the inner diameter was negligible and both the receptive field center and surround were modulated (upper plot). Increasing the diameter resulted in a sharp transition in response phase as the contribution of the center to the overall

response declined (lower plot). Response amplitude then rose with increasing diameter size until a pure surround response was attained (upper plot). Further increases in inner diameter size decreasingly modulated the receptive field, resulting in a decrease in response amplitude.

Finally, the spatial frequency response was measured using sinusoidal gratings drifted across the receptive field at 2 Hz (Fig. 4E). The response climbed to a peak amplitude near 1 cycle/deg and rolled of sharply at higher spatial frequencies (Fig. 4E, upper plot). The bandpass nature of the response is a classic feature of center-surround receptive field organization: at the lowest spatial frequencies response phase is intermediate between center and surround and spatial antagonism is maximal; at higher spatial frequencies only the receptive field center is responsive.

To estimate the dimensions of the center and surround we fit the spot, annulus, and spatial frequency response measurements with a difference of Gaussians model of the receptive field as described in Section 2. The model fit to the data are shown as the solid curves for both the amplitude and phase plots in Fig. 4C–E. Different parameter values were used to fit the three datasets yet the Gaussian diameters for both center (mean $\pm$ SD; 43 ± 8.5 μm) and surround (mean $\pm$ SD; 437 ± 61.9 μm) were in excellent agreement for all three datasets and are illustrated as a one dimensional plot of the center and surround Gaussians for this midget cell (Fig. 4F).

The spatial frequency response and difference of Gaussian fit for a diffuse bipolar cell is shown in Fig. 5 and a summary of the spatial dimensions of all the bipolar cells recorded using the DLP-based visual stimulator is given in Table 1. Receptive field dimensions were determined for eight diffuse and four midget bipolar cells. The four midget bipolar cells all had similar center diameters, ranging from about 30–50 μm. The diffuse bipolar cells all had center diameters that were about twice that of the midget bipolar cells, with a mean diameter of 92 μm (Table 1). For all cells the center diameters were larger than might be expected from the known morphology and cone connections of the diffuse and midget bipolar cell dendrites (Boycott & Wässle, 1991; Milam et al., 1993).

The surround diameters for both midget and diffuse bipolar cells were much larger than the centers, with a surround to center ratio consistently of ~ 9 (mean $\pm$ SD; 9.2 ± 2.4). The surround diameters for the midget bipolar cells tended to be about half that of the diffuse bipolar cells (Table 1). The ratio of surround to center strength derived from the Gaussian fits tended to be balanced at ~ 1 for most cells though there was some variability (mean $\pm$ SD; 1.3 ± 0.62), and for a few cells the surround was two to three times stronger than the center (Table 1).

4. Discussion

All of the primate cone bipolar cells recorded so far in vitro showed a strong and easily measured surround contribution to the spatial receptive field. By contrast in cat retina it has been reported that cone bipolar cells either totally lacked or showed very weak surrounds (Nelson et al., 1981; Nelson & Kolb, 1983). These earlier studies used narrow slits of light to probe for a surround and found evidence for a possible weak surround in only one out of nine cells recorded. The inability to observe the bipolar surround in cat retina may have been due to the technical difficulties of systematically recording from these small interneurons. In addition, these previous studies did not use an annular stimulus, which would have been the most effective for isolating the surround. The unequivocal bipolar surround observed in the primate retina in vitro probably reflects the precise targeting of bipolar cell bodies directly under fine microscopic control in vitro, giving a higher yield of good quality recordings from which a

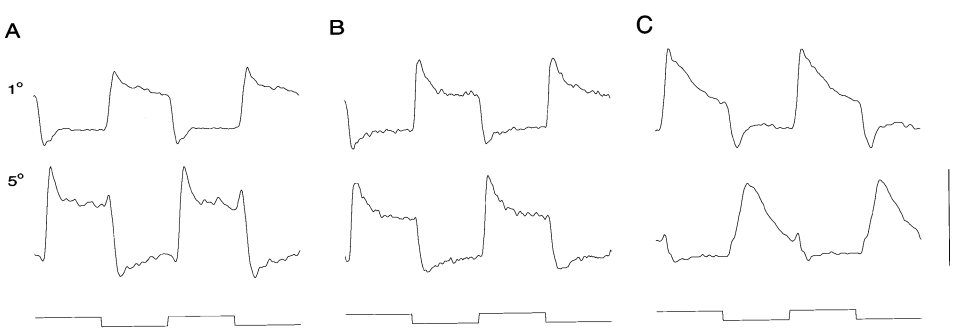

Fig. 3. Responses of three diffuse cone bipolar cells to 100% luminance contrast. (A–B) Two OFF-center bipolar cells hyperpolarized to a 1° diameter spot (upper traces) and depolarized to a 5° spot (lower traces). Temporal frequency was 2.44 Hz in A and 1.22 Hz in B. (C) ON-center bipolar cell depolarized to the 1° spot (upper trace) and hyperpolarized to the 5° spot (lower trace). Stimulus temporal frequency was 2.44 Hz. Scale bar = 6 mV for traces in A and 2 mV for traces in B & C. Stimulus waveform is shown below the traces.

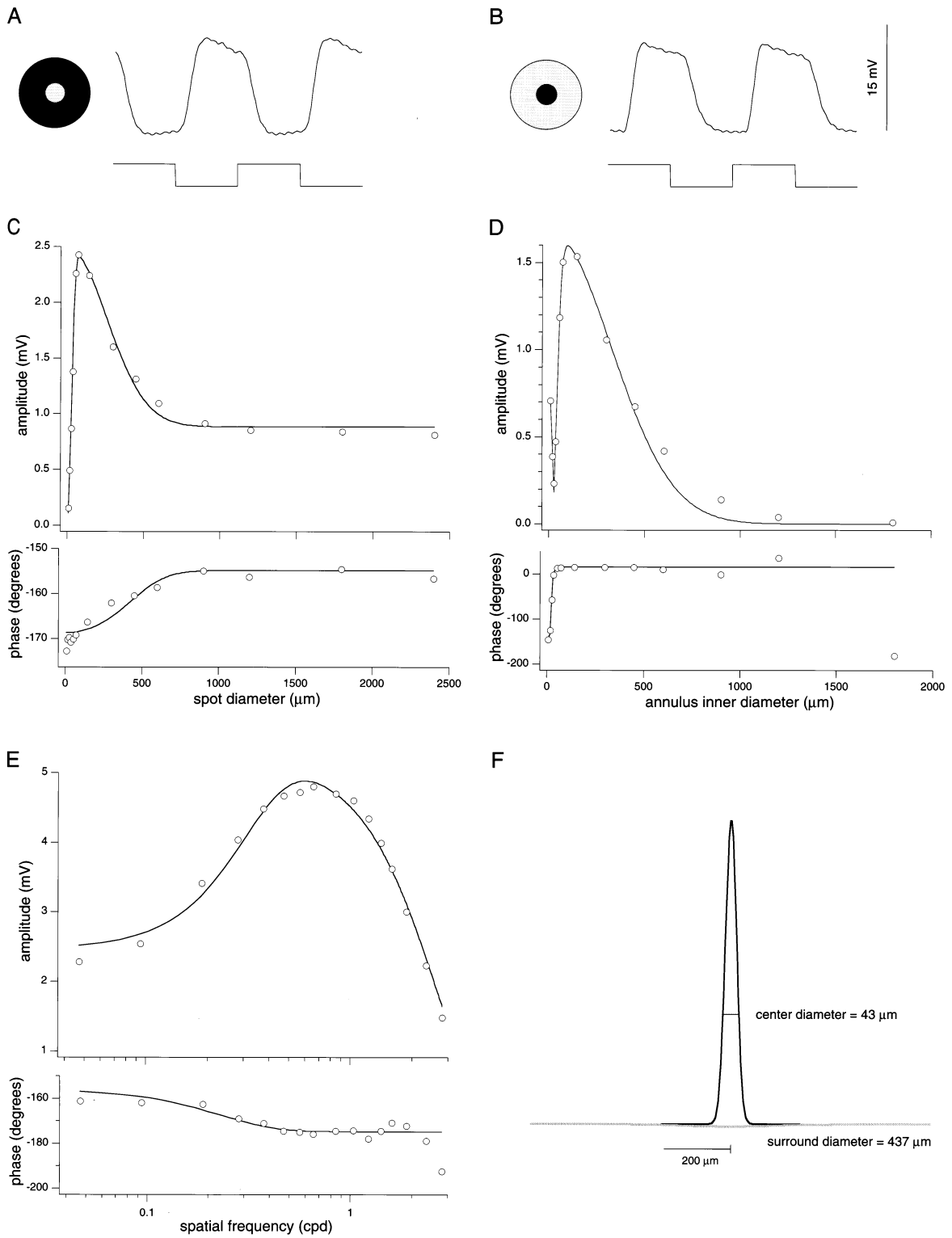

Fig. 4. Center-surround receptive field structure of an OFF-center midget bipolar cell. (A) Cell hyperpolarized to a small 150 μm diameter spot centered on the receptive field. (B) Cell depolarized to an annulus (inner diameter = 150 μm; outer diameter = 1200 μm). Stimulus waveform is shown below the traces in A and B. C–E. Responses of the same cell to flickering spots (2.44 Hz) of increasing size (C), flickering annuli (2.44 Hz) of increasing inner diameter (D), and sinusoidal gratings drifted across the receptive field at 2.44 Hz (E). All stimuli were centered on the receptive field and presented on a steady background of the same mean luminance as the stimuli (1000 td). Modulation contrast was 100%. Upper plots in C–E show response amplitude, lower plots show response phase. Solid lines in C–E are the difference of Gaussians model fits to the data as described in Section 2. Spatial frequency in E is given as cycles per degree (cpd) of visual angle for the macaque monkey eye (1 degree = 200 μm on the retina). (F) One dimensional plot of the center and surround Gaussians derived from the model fits shown in C-E, giving the center (43 μm) and surround (437 μm) mean receptive field diameters (diameter = 2x the Gaussian radius). The ratio of the surround to center weights for this cell was 0.7 (see Table 1, cell # A91199-6).

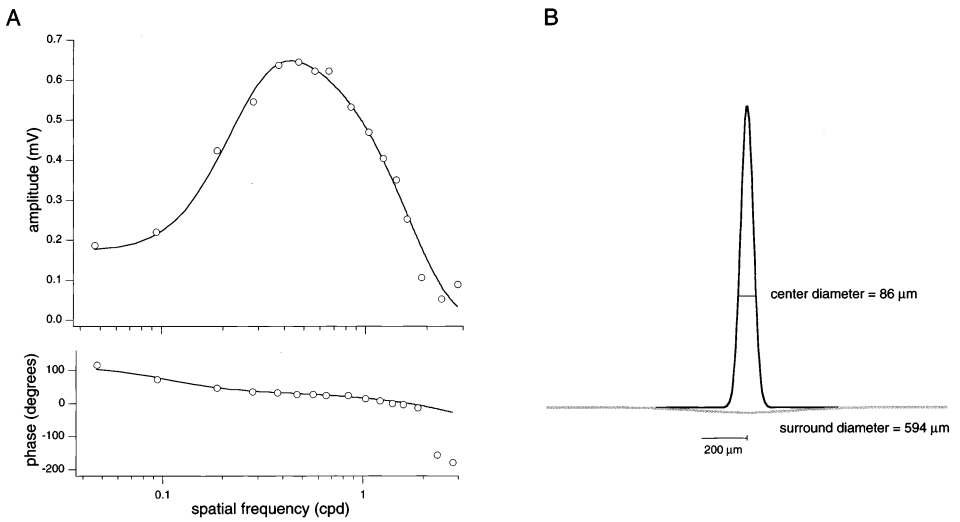

Fig. 5. Center-surround receptive field structure of an OFF-center diffuse bipolar cell. (A) Spatial frequency response to drifting (2.44 Hz) sinusoidal gratings of 100% contrast centered on the receptive field and presented on a steady background of the same mean luminance (1000 td). Upper plot shows response amplitude, lower plot shows response phase. Spatial frequency is given as cycles per degree (cpd) of visual angle for the macaque monkey eye (1° = 200 μm on the retina). Solid lines through the data are the difference of Gaussians model fits as described in Section 2. (B) Plot of the center and surround Gaussians derived from the model fit shown in A, giving the center (86 μm) and surround (594 μm) mean receptive field diameters. The ratio of the surround to center weights for this cell was 0.9 (see Table 1, cell # F96220-7).

variety of stimuli could be used to elicit a surround contribution. Under these recording conditions, bipolar cell receptive fields show an overall picture like that previously described in detail for a number of non-mammalian species (see Kaneko, 1983; Attwell, 1986; Poznanski & Umino, 1997 for reviews), and is consistent with other evidence predictive of a bipolar cell surround in mammals (Leeper & Charlton, 1985; Smith & Sterling, 1990; Cohen & Sterling, 1991; Vardi, Masarachia & Sterling, 1992; Greferath, Grünert, Müller & Wässle, 1994; Vardi & Sterling, 1994). Measurements of receptive field dimensions using a difference of Gaussians model fit to the spatial frequency response or to discrete spots and annuli provided an excellent fit to the data and yielded center and surround properties comparable to that described for bipolar cells of the tiger salamander retina using comparable techniques (e.g. Hare & Owen, 1990).

How do our estimates of cone bipolar cell center and surround dimensions fit with current understanding of the morphology and circuitry of the diffuse and midget bipolar cell classes (and with the receptive field dimensions of the ganglion cells whose light response they must largely determine)? The receptive field centers of both the diffuse and midget bipolar cells in our sample are larger than expected from the known number of cone inputs to their dendritic trees (Boycott & Wässle, 1991). In peripheral retina diffuse bipolar cells contact from 5–10 cones, giving an anatomical diameter of about 30–50 μm, but the eight diffuse bipolar cells measured here showed receptive field centers averaging about 90 μm, that would suggest input from ~20–30 cones. For midget bipolar cells, it is known that at retinal eccentricities up to 10 mm virtually all cells restrict dendritic contact to single cones (Milam et al., 1993; Wässle et al., 1994); this was confirmed for the cell whose light response is illustrated in Fig. 4. By contrast the receptive field center diameters of these cells are in the range of 40 μm which would encompass ~5–10 cones.

Table 1
Center and surround receptive field sizes of diffuse and midget bipolar cells of the macaque retina

Cell type	Cell #	Eccentricity (mm from fovea)	Mean center diameter[a] (μm)	Mean surround diameter[a] (μm)	Surround/center weights
Midget	94071-4	10.0	51	515	1.0
	T96219-5	8.0	41	432	0.9
	A91199-6	13.6	43	437	0.7
	F93148-3	~14	31	438	1.1
All midgets			42	467	
Diffuse	F88048-5	~14	101	1048	1.7
	F88048-6	~14	103	723	0.8
	94071-3	9.8	100	788	1.3
	F96220-7	10.5	86	594	0.9
	F96220-9	10.3	79	602	2.0
	A91199-4	12.6	83	665	2.8
	A91199-5	13.0	74	612	0.8
	90059-2	8.6	114	914	1.3
All diffuse			92	743	

[a] Diameter = 2× the Gaussian radius.

The basis for the apparently large receptive field center size cannot be due to the optical quality of the stimulus incident on the retina, which would be satisfactory for measuring higher spatial frequency cutoffs than was found for the recorded cone bipolar cells (Fig. 1B). Whether the stimulus quality is somehow further degraded in the in vitro preparation as it traverses the retina to reach the cone outer segments cannot at this time be ruled out. Any potential blur in the in vitro preparation, however, would not affect the measurements of the larger receptive fields of the diffuse cone bipolar cells, and we were able to measure relatively small receptive fields in midget bipolar cells (Table 1). Our data are also in line with the finding that parafoveal ganglion cells of the midget pathway, which receive all of their bipolar cell input from a single midget bipolar cell, also consistently show receptive fields larger than would be expected from input driven by a single cone (Derrington & Lennie, 1984; Croner & Kaplan, 1995; review: Lee, 1999). Indeed, the receptive field diameters of the four peripheral midget bipolar cells fall within or very close to that found for parafoveal midget ganglion cells using similar stimuli. By contrast, the receptive field centers for midget ganglion cells in far retinal periphery are two to three times larger in diameter than that shown here for midget bipolar cells (Croner & Kaplan, 1995; Dacey, 1999). Similarly, the parasol ganglion cells also have receptive field centers (Croner & Kaplan, 1995) that are two to three times that found for the diffuse cells, their source of bipolar input (Calkins, 1999). Thus for both the midget and diffuse cone bipolar cells, center sizes are consistent with the expectation that, in the retinal periphery at least, convergent input from several bipolar cells determines the extent of the ganglion cell receptive field center.

Our data also fit with the finding that the receptive field center sizes of bipolar cells in non-mammalian retina are also enlarged relative to the size of the dendritic tree (reviews: Vaney, 1994; Poznanski & Umino, 1997). However in the non-mammalian case the bipolar receptive field center is an order of magnitude larger than the dendritic tree, reaching in some instances ~ 1000 μm in diameter and it is clear that these bipolar cells form extended, electrically coupled networks like that long recognized for horizontal cells (Kujiraoka & Saito, 1986; Borges & Wilson, 1990; Hare & Owen, 1990; Poznanski & Umino, 1997). Clearly this kind of strong electrical coupling does not occur in the primate bipolar cell but it is possible that some electrical coupling among neighboring bipolar cells and/or cones in primate may account for the full extent of the receptive field center: both cone–cone (e.g. Raviola & Gilula, 1973; Tsukamoto, Masarachia, Schein & Sterling, 1992), and bipolar–bipolar cell gap junctions have been observed in mammalian retina (Kolb, 1979). The homotypic tracer coupling found for the diffuse bipolar cell shown in Fig. 2 most likely occurs via gap junctions and is consistent with this hypothesis.

The size and relative strength of the surrounds of the diffuse and midget bipolar cells are very similar to those measured with similar stimuli for the parasol and midget ganglion cell classes in the retinal periphery (Croner & Kaplan, 1995). The balance of surround and center strength is generally similar, though not matching, for the bipolar and ganglion cells. Both bipolar and ganglion cells show a surround/center gain ratio of about 1, but the bipolar cells tend to be more surround dominated (mean ratio = 1.3) than the ganglion cells (mean ratio = 0.55) (Croner & Kaplan, 1995). For the bipolar cells, the ratio of surround to center diameter is consistently ~ 10; at the ganglion cell level there is some variability but the surrounds for most midget and parasol ganglion cells were only about 2–5 larger than the center (Croner & Kaplan, 1995). Clearly a larger database of bipolar cell receptive fields will be needed to look at the transformation in the relative size and gain of the center to surround from bipolar cell to ganglion cell.

Though we are only at the beginning of an understanding of the physiology of primate bipolar cells, these initial results suggest that the basic spatial structure of the ganglion cell receptive field is established at the level of the bipolar cell. Although recent experiments in rabbit retina suggest that spiking amacrine cells largely establish the surrounds of at least some ganglion cells (Taylor, 1999), the precise role that amacrine cells play in creating the ganglion cell surround remains to be clarified. In primates the diffuse bipolar-parasol pathway may be distinguished from the midget pathway by a higher percentage of amacrine cell input (Kolb & Dekorver, 1991; Jacoby, Stafford, Kouyama & Marshak, 1996). This anatomical distinction may be related to the consistent difference in surround diameters for the midget and diffuse bipolar cells. For the midget bipolar cells, the surrounds are about the same as the receptive field diameters of macaque H1 horizontal cells measured using the same techniques at the same retinal locations (Dacey, 2000), supporting the classical view that this bipolar cell surround is derived largely via the circuitry of the outer retina. The diffuse bipolar cell surrounds are consistently larger, suggesting a role for input from a large field amacrine cell type in the full extent of the surround.

Acknowledgements

Supported by NIH grants EY06678, EY09625 (DMD), EYO1730 (Vision Research Core) and

RR00166 to the Regional Primate Research Center at the University of Washington. Toni Haun and Keith Boro provided technical assistance.

References

Attwell, D. (1986). Ion channels and signal processing in the outer retina. *Quarterly Journal of Experimental Physiology*, *71*, 713–739.

Barlow, H. B. (1953). Action potentials from the frog's retina. *Journal of Physiology*, *119*, 58–68.

Barlow, H. B. (1961). Possible principles underlying the transformation of sensory messages. In W. A. Rosenblith, *Sensory communication* (pp. 217–234). Cambridge: MIT Press.

Borges, S., & Wilson, M. (1990). The lateral spread of signal between bipolar cells of the tiger salamander retina. *Biological Cybernetics*, *63*, 45–50.

Boycott, B. B., & Dowling, J. E. (1969). Organization of the primate retina: light microscopy. *Philosophical Transactions of the Royal Society of London B*, *Biological Science*, *255*, 109–184.

Boycott, B. B., & Wässle, H. (1991). Morphological classification of bipolar cells of the primate retina. *European Journal of Neuroscience*, *3*, 1069–1088.

Burkhardt, D. A. (1993). Synaptic feedback, depolarization, and color opponency in cone photoreceptors. *Visual Neuroscience*, *10*, 981–989.

Calkins, D. J. (1999). Synaptic organization of cone pathways in the primate retina. In K. Gegenfurtner, & L. Sharpe, *Color vision from molecular genetics to perception*. Cambridge University Press, Cambridge (in press).

Calkins, D. J., Schein, S. J., Tsukamoto, Y., & Sterling, P. (1994). M and L cones in macaque fovea connect to midget ganglion cells by different numbers of excitatory synapses. *Nature*, *371*, 70–72.

Cohen, E.., & Sterling, P. (1991). Microcircuitry related to the receptive field center of the On-beta ganglion cell. *Journal of Neurophysiology*, *65*, 352–359.

Croner, L. J., & Kaplan, E. (1995). Receptive fields of P and M ganglion cells across the primate retina. *Vision Research*, *35*, 7–24.

Dacey, D. M. (1999). Primate retina: cell types, circuits and color opponency. *Progress in Retinal Research*, *18* (in press).

Dacey, D. M. (2000). Parallel pathways for spectral coding in primate retina. *Annual Review of Neuroscience*, *23* (in press).

Dacey, D. M., & Lee, B. B. (1994). The blue-ON opponent pathway in primate retina originates from a distinct bistratified ganglion cell type. *Nature*, *367*, 731–735.

Dacey, D. M., Lee, B. B., Stafford, D. K., Pokorny, J., & Smith, V. C. (1996). Horizontal cells of the primate retina: cone specificity without spectral opponency. *Science*, *271*, 656–659.

Dacheux, R. F., & Miller, R. F. (1981). An intracellular electrophysiological study of the ontogeny of functional synapses in the rabbit retina. I. Receptors, horizontal, and bipolar cells. *Journal of Comparative Neurology*, *198*, 307–326.

Dacheux, R. F., & Raviola, E. (1986). The rod pathway in the rabbit retina. A depolarizing bipolar and amacrine cell. *Journal of Neuroscience*, *6*, 331–345.

Derrington, A. M., & Lennie, P. (1984). Spatial and temporal contrast sensitivities of neurons in lateral geniculate nucleus of macaque. *Journal of Physiology*, *357*, 219–240.

Enroth-Cugell, C., Robson, J. G., Schweitzer-Tong, D. E., & Watson, A. B. (1983). Spatio–temporal interactions in cat retinal ganglion cells showing linear spatial summation. *Journal of Physiology* (*London*), *341*, 279–307.

Grace, A. (1990). *Optimization toolbox for use with Matlab: User's Guide*. Natlick, MA: The Mathworks, Inc.

Greferath, U., Grünert, U., Müller, F., & Wässle, H. (1994). Localization of $GABA_A$ receptors in the rabbit retina. *Cell Tissue Research*, *276*, 295–307.

Grünert, U., Martin, P. R., & Wässle, H. (1994). Immunocytochemical analysis of bipolar cells in the macaque monkey retina. *Journal of Comparative Neurology*, *348*, 607–627.

Hare, W. A., & Owen, W. G. (1990). Spatial organization of the bipolar cell's receptive field in the retina of the tiger salamander. *Journal of Physiology* (*London*), *421*, 223–245.

Jacoby, R., Stafford, D., Kouyama, N., & Marshak, D. (1996). Synaptic inputs to ON parasol ganglion cells in the primate retina. *Journal of Neuroscience*, *16*, 8041–8156.

Kamermans, M., & Spekreijse, H. (1999). The feedback pathway from horizontal cells to cones — A mini review with a look ahead. *Vision Research*, *39*, 2449–2468.

Kaneko, A. (1973). Receptive field organization of bipolar and amacrine cells in the goldfish retina. *Journal of Physiology* (*London*), *235*, 133–153.

Kaneko, A. (1983). Retina bipolar cells: their function and morphology. *Trends in Neuroscience*, *6*, 219–223.

Kolb, H. (1979). The inner plexiform layer in the retina of the cat: electron microscopic observations. *Journal of Neurocytology*, *8*, 295–329.

Kolb, H., & Dekorver, L. (1991). Midget ganglion cells of the parafovea of the human retina: a study by electron microscopy and serial section reconstructions. *Journal of Comparative Neurology*, *303*, 617–636.

Kouyama, N., & Marshak, D. W. (1992). Bipolar cells specific for blue cones in the macaque retina. *Journal of Neuroscience*, *12*, 1233–1252.

Kuffler, S. W. (1953). Discharge patterns and functional organization of mammalian retina. *Journal of Neurophysiology*, *16*, 37–68.

Kujiraoka, T., & Saito, T. (1986). Electrical coupling between bipolar cells in carp retina. *Proceedings of the National Academy of Sciences USA*, *83*, 4063–4066.

Lee, B. B. (1999). Receptor inputs to primate ganglion cells. In K. R. Gegenfurtner, & L. T. Sharpe, *Color vision: from genes to perception* (pp. 203–218). New York: Cambridge University Press.

Leeper, H. F., & Charlton, J. S. (1985). Response properties of horizontal cells and photoreceptor cells in the retina of the tree squirrel, *Sciurus carolinensis*. *Journal of Neurophysiology*, *54*, 1157–1166.

Mangel, S. C. (1991). Analysis of the horizontal cell contribution to the receptive field surround of ganglion cells in the rabbit retina. *Journal of Physiology* (*London*), *442*, 211–234.

Mariani, A. P. (1984). Bipolar cells in monkey retina selective for the cones likely to be blue-sensitive. *Nature*, *308*, 184–186.

Matsumoto, N., & Naka, K. I. (1972). Identification of intracellular responses in the frog retina. *Brain Research*, *42*, 59–71.

Milam, A. H., Dacey, D. M., & Dizhoor, A. M. (1993). Recoverin immunoreactivity in mammalian cone bipolar cells. *Visual Neuroscience*, *10*, 1–12.

Nelson, R., & Kolb, H. (1983). Synaptic patterns and response properties of bipolar and ganglion cells in the cat retina. *Vision Research*, *23*, 1183–1195.

Nelson, R., Kolb, H., Robinson, M. M., & Mariani, A. P. (1981). Neural circuitry of the cat retina: cone pathways to ganglion cells. *Vision Research*, *21*, 1527–1536.

Packer, O. S., Diller, L., Brainard, D., & Dacey, D. M. (2000). Characterization and use of a digital light projector for vision research. *Journal of the Optical Society of America* (submitted).

Polyak, S. L. (1941). *The retina*. Chicago: University of Chicago Press.

Poznanski, R. R., & Umino, O. (1997). Syncytial integration by a network of coupled bipolar cells in the retina. *Progress in Neurobiology*, *53*, 273–291.

Raviola, E., & Gilula, N. B. (1973). Gap junctions between photoreceptor cells in the vertebrate retina. *Proceedings of the National Academy of Sciences USA*, *70*, 1677–1681.

Rodieck, R. W., & Stone, J. (1965). Analysis of receptive fields of cat retinal ganglion cells. *Journal of Neurophysiology*, *28*, 833–849.

Schwartz, E. A. (1974). Response of bipolar cells in the retina of the turtle. *Journal of Physiology* (*London*), *236*, 211–224.

Srinivasan, M. V., Laughlin, S. B., & Dubs, A. (1982). Predictive coding: a fresh view of inhibition in the retina. *Proceedings of the Royal Society of London*, *B*, *216*, 427–459.

Smith, R. G., & Sterling, P. (1990). Cone receptive field in cat retina computed from microcircuitry. *Visual Neuroscience*, *5*, 453–461.

Taylor, W. R. (1999). TTX attenuates surround inhibition in rabbit retinal ganglion cells. *Visual Neuroscience*, *16*, 285–290.

Tsukamoto, Y., Masarachia, P., Schein, S., & Sterling, P. (1992). Gap junctions between the pedicles of macaque foveal cones. *Vision Research*, *32*, 1809–1815.

Vaney, D. I. (1994). Patterns of neuronal coupling in the retina. In *Progress in retinal and eye research* (pp. 301–355). UK: Pergamon.

Vardi, N., Masarachia, P., & Sterling, P. (1992). Immunoreactivity to $GABA_A$ receptor in the outer plexiform layer of the cat retina. *Journal of Comparative Neurology*, *320*, 394–397.

Vardi, N., & Sterling, P. (1994). Subcellular localization of $GABA_A$ receptor on bipolar cells in macaque and human retina. *Vision Research*, *34*, 1235–1246.

Werblin, F. S., & Dowling, J. E. (1969). Organization of the retina of the mudpuppy, *Necturus maculosus*. II. Intracellular recording. *Journal of Neurophysiology*, *32*, 339–355.